High Pressure Research

ISSN: 0895-7959 (Print) 1477-2299 (Online) Journal homepage: https://www.tandfonline.com/loi/ghpr20

Single-crystal X-ray diffraction at megabar pressures and temperatures of thousands of degrees

L. Dubrovinsky , T. Boffa-Ballaran , K. Glazyrin , A. Kurnosov , D. Frost , M. Merlini , M. Hanfland , V. B. Prakapenka , P. Schouwink , T. Pippinger & N. Dubrovinskaia

To cite this article: L. Dubrovinsky , T. Boffa-Ballaran , K. Glazyrin , A. Kurnosov , D. Frost , M. Merlini , M. Hanfland , V. B. Prakapenka , P. Schouwink , T. Pippinger & N. Dubrovinskaia (2010) Single-crystal X-ray diffraction at megabar pressures and temperatures of thousands of degrees, High Pressure Research, 30:4, 620-633, DOI: 10.1080/08957959.2010.534092

To link to this article: https://doi.org/10.1080/08957959.2010.534092

High Pressure Research
Vol. 30, No. 4, December 2010, 620–633

Taylor & Francis
Taylor & Francis Group

Single-crystal X-ray diffraction at megabar pressures and temperatures of thousands of degrees

L. Dubrovinsky[a]*, T. Boffa-Ballaran[a], K. Glazyrin[a], A. Kurnosov[a], D. Frost[a], M. Merlini[b,c], M. Hanfland[c], V.B. Prakapenka[d], P. Schouwink[e], T. Pippinger[e] and N. Dubrovinskaia[e,f]

[a]Bayerisches Geoinstitut, Universität Bayreuth, 95440 Bayreuth, Germany; [b]Dipartimento di Scienze della Terra, Università degli Studi di Milano, Via Botticelli 23, 20133 Milano, Italy; [c]ESRF, Boîte Postale 220, 38043 Grenoble, France; [d]GeoSoilEnviroCARS, University of Chicago, 5640 South Ellis, Chicago, IL 60637, USA; [e]Mineralphysik, Institut für Geowissenschaften, Universität Heidelberg, 69120 Heidelberg, Germany; [f]Lehrstuhl für Kristallographie, Physikalisches Institut, Universität Bayreuth, 95440 Bayreuth, Germany

(*Receieved 17 October 2010; final version received 19 October 2010*)

The most reliable information about crystal structures and their response to changes in pressure and temperature is obtained from single-crystal diffraction experiments. We have developed a methodology to perform single-crystal X-ray diffraction experiments in laser-heated diamond anvil cells and demonstrate that structural refinements and accurate measurements of the thermal equation of state of metals, oxides and silicates from single-crystal intensity data are possible in pressures ranging up to megabars and temperatures of thousands of degrees. A new methodology was applied to solve the *in situ* high pressure, high temperature structure of iron oxide and study structural variations of iron and aluminum bearing silicate perovskite at conditions of the Earth's lower mantle.

Keywords: single-crystal diffraction; laser heating; diamond anvil cells; silicate perovskite; tungsten; iron oxide

1. Introduction

Since its first applications in the late 1950s, the diamond anvil cell (DAC) technique has become the most successful method for generating high pressure conditions, providing the opportunity for high pressure researchers to study matter at pressures above 300 GPa using a wide range of different techniques, *i.e.* Mössbauer, infrared and Raman spectroscopy, as well as resistivity, X-ray diffraction and inelastic scattering measurements [1–9]. In particular, single-crystal X-ray diffraction of samples loaded in DACs provide the most reliable data to determine the equation of state and structural changes of materials at elevated pressures [9,10]. The development of miniature DACs with a large optical opening (above 60°) [1,11], fast two-dimensional area detectors and bright X-ray sources (*i.e. in-house* rotating anodes and synchrotron radiation facilities [9]) are

*Corresponding author. Email: leonid.dubrovinsky@uni-bayreuth.de

ISSN 0895-7959 print/ISSN 1477-2299 online

DOI: 10.1080/08957959.2010.534092
http://www.informaworld.com

the basis of the drastic progress in high pressure crystallography. However, the high quality of single crystals is very difficult to maintain in the harsh environment of DAC experiments, having inhomogeneous pressure distribution, as well as differential and shear stresses as a negative effect, and until recently, the freezing point of fluid pressure-transmitting media (10–15 GPa [12]) defined the limits of X-ray single-crystal diffraction experiments in DACs. Advances in methods of noble gas loading (especially neon and helium) [8,13] at pressures of 0.1–0.2 GPa have made it possible to preserve the high quality of single crystals in DACs even at 100 GPa or above [2,6,14] at ambient temperatures. However, the field of a single-crystal study at simultaneously high pressures and high temperatures is still to be explored.

2. Portable laser-heating system for single-crystal X-ray diffraction experiments in DACs

There are two major methods of heating in DACs: laser and electric [8,11]. X-ray powder diffraction experiments under electric (external) heating in DACs are possible at temperatures up to about 1200 K and over 250 GPa [11,15]; however, single-crystal studies are limited to about $\sim$1000 K [5,16]. Laser-heating techniques in DACs cover a wide pressure–temperature field – above 300 GPa and up to 5000 K [8,18,19]. Recent advantages in online laser-heating techniques [17] have resulted in significant improvement of the reliability of *in situ* X-ray powder diffraction studies in laser-heated DACs that have become routine at a number of synchrotron facilities including specialized beamlines at the third-generation synchrotrons. However, so far, no existing DAC laser-heating systems can be used for single-crystal X-ray diffraction experiments aimed not only at determining lattice parameters, but also at measuring intensity data for structural refinements. The reason for this is that in all existing DAC laser-heating facilities, the laser beam enters the cell at a fixed angle, and a partial rotation of the DAC, as required in monochromatic single-crystal X-ray diffraction experiments, results in the loss of the target and may be even dangerous if the powerful laser light starts to scatter in arbitrary directions by the diamond anvils. In order to overcome this problem, we have modified a portable laser-heating system according to our own design [19].

The system consists of two major components – the source of laser light (100 W SPI100 Modulated High-Power Fiber Laser) and the universal laser-heating head (UniHead) (Figure 1). The functions of the UniHead in the portable laser heating system are: (1) to focus the incoming laser beam on the sample within the DAC; (2) to provide a high magnification imaging of the sample in the DAC with coaxial illumination; and (3) to give access for the multiwavelength spectroradiometry for temperature measurements [19]. The output of the SPI100 laser has a Gaussian shape with a diameter of $\sim$3 mm at $1/e^2$ and is focused down to $\sim$25 μm at FWHM, while if the π-shaper [17] is used (Figure 1), the beam size increases to $\sim$40 μm and forms a flat top. Due to the modular construction, the portable laser-heating system can be used in various modifications; namely, for heating samples in an independently standing DAC or in a cell coupled directly to UniHead – in a "direct" (the optical axis of the DAC and the UniHead axis coincide) or "right angle" (at 90° between the optical axis of the DAC and that of the UniHead) geometry. In the following experiments performed at the ID09a beamline at the ESRF synchrotron facility, we employed the UniHead in the "right angle" geometry with a carbon mirror mounted from the side of the incident X-ray beam (inset in Figure 1). The X-ray scattering from glassy carbon, which has been used as a substrate for the silver coating, was blocked by the DAC's body and did not introduce any features into the X-ray diffraction profiles. In the "right angle" geometry, the DAC and the UniHead, mounted on a common general platform, were rotated simultaneously, and ω-scans (necessary for single-crystal X-ray diffraction experiments) were realized without loss of focusing of the laser. In the present configuration, we used ω-scans in the range of $-30°$ to $+10°$ with a 0.5° step size.

Figure 1. Universal laser-heating head (UniHead) (1) with a π-shaper (2) mounted for single-crystal X-ray diffraction experiments in DAC at the ID09a beamline at ESRF (Grenoble). (3) The optical fiber connected to the 100 W laser light source, (4) the silver-coated carbon mirror, (5) the DAC (green arrow in inset shows the direction of the laser beam; color online).

We demonstrate the application of this system for simultaneous high pressure and high temperature single-crystal diffraction studies using three examples – accurate measurements of the lattice parameters of tungsten single crystals at pressures up to 43 GPa and 2500 K and high pressure, high temperature structural behavior of hematite Fe_2O_3 and silicate perovskite $(Mg_{0.62},Fe_{0.38})(Al_{0.36}Si_{0.64})O_3$ at conditions of the Earth's lower mantle.

3. Experimental

3.1. *Samples preparations*

Single crystals of tungsten of 99.999% purity with the size of about $10 \times 10 \times 10\,\mu m^3$ were provided by Goodfellow Inc. Single crystals of hematite Fe_2O_3 were synthesized by the slow

oxidation of pure (99.999%) iron at 1200 °C in a gas-mixing furnace at BGI. For experiments in DACs small ($\sim 15 \times 15 \times 5\,\mu m^3$), crystals were selected and tested using the *in-house* Xcalibur™ diffractometer.

A single crystal of $(Mg_{0.62},Fe_{0.38})(Al_{0.36}Si_{0.64})O_3$ silicate perovskite was synthesized in a multi-anvil apparatus at 25 GPa and 1300 °C. The chemical composition was determined from microprobe analysis. According to the Mössbauer spectroscopy data, $Fe^{3+}/\Sigma Fe \sim 0.9$ (C. McCammon, pers. comm.). Single crystals of up to $50 \times 40 \times 20\,\mu m^3$ size were selected and tested before loading into a DAC using *in-house* Xcalibur™ diffractometer.

3.2. *DAC experiments*

In different runs, the sample was clamped between the diamond anvils with culets of 300 or 250 μm in diameter. Rhenium gaskets were indented to the thickness of about 50 μm and holes with a diameter of 100–150 μm were drilled in the center. Single crystals (one per run) of the investigated material were loaded into the holes, along with ruby spheres as pressure markers. Ne was loaded at 1.4 kbar both as a pressure-transmitting medium and an internal pressure standard.

3.3. *Single-crystal diffraction*

All single-crystal high pressure laser-heated DAC experiments were conducted at ID09a at the European Synchrotron Radiation Facility (ESRF). Diffraction data were collected at 293 K using the MAR555 Flatpanel detector, radiation with a wavelength of 0.4153 Å, beam size $10 \times 10\,\mu m^2$ and the crystal-to-detector distance of about 399 mm. Eighty frames in the ω-scanning range of $-30°$ to $+10°$ were collected (0.5° scanning step size) with the exposure time of 1 s. The data were processed using the CrysAlis® software (Oxford Diffraction (2006) CrysAlis RED, Version 1.171.31.8. Oxford Diffraction Ltd, Abingdon, Oxfordshire, UK). Crystal structure refinements of integrated intensities were carried out with the SHELXL-97 WinGX version [20].

4. Results and discussions

4.1. *Thermal EOS of tungsten*

High pressure research depends critically on pressure standards. The common requirements for the pressure standard are a simple crystal structure giving few diffraction lines, the absence of phase transitions at high pressures and temperatures and relative chemical stability. Tungsten naturally satisfies these conditions and its accurate equation of state at ambient temperature has already been measured, based on single-crystal compression experiments up to above 150 GPa [21]. There are theoretical predictions on the thermal equation of state (EOS) of tungsten (see [22] and references therein), but experimental static compression data at high temperatures are lacking. We determined the lattice parameters of tungsten single crystals compressed in an Ne pressure-transmitting medium (which can also be used as an internal pressure standard [23]; Figure 2). Because of the simple body-centered cubic structure with just two atoms per unit cell, usually only three to five powder diffraction lines can be measured in high pressure experiments and X-ray energy up to 40 keV, whereas using a single crystal, 8–16 diffraction peaks were recorded and individually integrated after refining the beam center position. The fit of 15 P–V data points collected at ambient temperature and pressures between 4.5 and 46.6 GPa using the third-order Birch–Murnaghan EOS gave the bulk modulus of $K_{300} = 304(2)$ GPa and its pressure derivative of $K' = 4.1(2)$, in good agreement with the literature data [21] (Figure 3 and

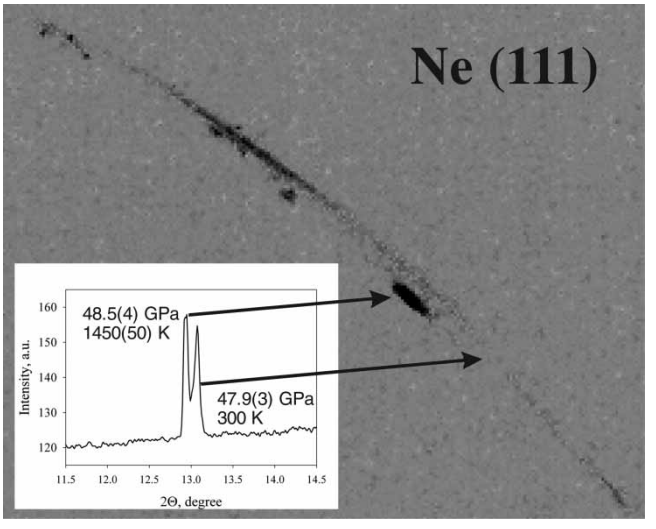

Figure 2. Splitting of the Ne (111) line during heating at 48 GPa. Pressure was calculated according to [23].

Table 1. Thermoelastic parameters of tungsten (Equations 1–3).

V_0 (Å^3/mol)	31.69(2)
$K'_{300,0}$	4.09(33)
α_1 (10^{-5} K^{-1})	1.37(1)
α_2 (10^{-9} K^{-2})	−0.74(2)
α_3 (K)	1.098(3)
b_1 (10^{-3} GPa^{-1})	3.168(28)
b_2 (10^{-7} K^{-1} GPa^{-1})	2.800(25)
b_3 (10^{-11} K^{-2} GPa^{-1})	−3.66(3)

Table 1). The data collected during laser heating were evaluated using a previously-described formalism [15]. Particularly, we used the following formula to describe our experimental data:

$$P = 1.5K_{T,0}\left[\left(\frac{\mathrm{V}_{T,0}}{V}\right)^{7/3} - \left(\frac{\mathrm{V}_{T,0}}{V}\right)^{5/3}\right]\left[1 - 0.75(4 - K'_{T,0})\left\{\left(\frac{\mathrm{V}_{T,0}}{V}\right)^{2/3} - 1\right\}\right], \quad (1)$$

where $K_{T,0}$, $K'_{T,0}$ and $V_{T,0}$ are the bulk modulus, its pressure derivative and the volume of the unit cell at zero pressure and temperature T (in K), respectively,

$$K_{T,0} = \frac{1}{b_1 + b_2 T + b_3 T^2}. \quad (2)$$

The unit cell volume $V_{T,0}$ is given by the following equation:

$$V_{T,0} = V_0 \exp\left(a_1 * (T - T_0) + \frac{a_2 * (T^2 - T_0^2)}{2} - c\left(\frac{1}{T} - \frac{1}{T_0}\right)\right), \quad (3)$$

where V_0 is the unit cell volume at zero pressure and b_i and α_i are parameters.

Figure 3 shows that the present results are in good agreement with *ab initio* predictions [22], raising confidence in both experimental and theoretical methodologies.

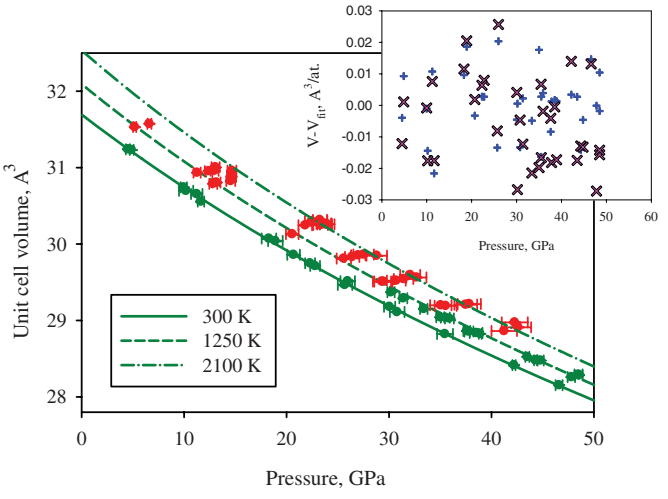

Figure 3. Unit cell volume of tungsten measured at different pressures and temperatures. The green data points were used to fit a thermal equation of state with Ne as a pressure gauge [23], as described by Equations (1)–(3) [15]. The pressures of the red data points and for the curves were determined using the fitted thermal EOS parameters. The inset shows the difference between the values of the measured unit cell volumes and the values obtained from the thermal equations of state in the present study (blue plus symbols) and the values predicted based on *ab initio* calculations (pink crosses) [22] (color online).

4.2. *Structure of a high pressure Fe_2O_3 polymorph*

At ambient pressure trigonal hematite α-Fe_2O_3 (space group $R\bar{3}c$) is a wide-gap antiferromagnetic insulator and can be considered as an archetype of a Mott-insulator [24]. Due to its significance in the solid state and mineral physics, the high pressure behavior of Fe_2O_3 has been intensively investigated (see [25–27] and references therein). On compression at ambient temperature above 50 GPa, it undergoes a sluggish structural phase transition [24–26] into a phase with an orthorhombic symmetry. The same phase has been reported [25] to appear upon heating above about 30 GPa. The exact structure of the orthorhombic phase remains, however, controversial. Two structural models have been proposed [24–26] – that of the high pressure Rh_2O_3-II-type structure (space group *Pbna*, #60) and the orthorhombic perovskite-type structure (space group *Pbnm*, #62). While the Mössbauer spectroscopic data seem to support the Rh_2O_3-II-type structure, the powder diffraction data collected by different groups at different synchrotron facilities over the last several decades were not able to unambiguously assign the structural type (see references in [24–26]). We compressed a single crystal of hematite Fe_2O_3 in a DAC loaded with Ne as the pressure-transmitting medium to 25.6(5) GPa and collected the X-ray diffraction data in 40° ω-scans with a 0.5° step. After integration of the intensity data collected, we obtained 45 unique reflections for the refinements of four structural parameters of hematite which resulted in a discrepancy index R1 = 4.5% (Table 2). Upon heating to 2200(100) K, the pressure increased to 34.0(5) GPa, the quality of the crystal decreased, but we still could collect 26 unique reflections with which we could refine the hematite structure with a 8.7% discrepancy factor (Table 2). Laser-heating at 40.4(5) GPa and 2300(100) K resulted in the appearance of a new set of reflections. All 50 unique reflections of this set were indexed with an orthorhombic unit cell with lattice parameters $a = 4.855(1)$ Å, $b = 5.039(2)$ Å and $c = 7.187(2)$ Å. The space group suggested by the CrysAlis® software was *Pbna*. This assignment is in consistency with the Rh_2O_3-II-type structure, and indeed, the 10 structural parameters related to this structure type could be refined with a discrepancy factor R1 = 5.2%. In contrast, the orthorhombic perovskite structural model (space group *Pbnm*, 11 refined structural parameters) gives a discrepancy factor of four times

Table 2. Results of single crystal structural refinement of Fe_2O_3 at different pressures and temperatures.

					Lattice parameters				
P (GPa)	*T* (K)	Structural type	Space group	R1 (%)	*a* (Å)	*B* (Å)	*C* (Å)	*V* (Å^3/formula)	Atomic parameters (*xyzU*)
25.6(2)	298	Hematite	$R\bar{3}c$	4.5	4.898(2)		13.196(10)	45.70(1)	Fe: 0 0 0.3561(2) 0.014(1); O: 0.3082(9) 0 0 0.017(2)
34.0(5)	2200(100)	Hematite	$R\bar{3}c$	8.7	4.906(3)		13.171(10)	45.75(2)	Fe: 0 0 0.3602(5) 0.095(4); O: 0.303(3) 0 0 0.12(1)
40.4(5)	2300(100)	Rh_2O_3-II	*Pbna*	5.2	4.855(1)	5.039(1)	7.187(2)	43.96(1)	Fe: 0.7522(2) 0.0314(7) 0.1168(7) 0.046(2); O1: 0.603(2) 0.098(2) 0.839(4) 0.077(4); O2: 0.069(2) 0.25 0 0.075(5)
40.4(5)	2300(100)	Orthorombic perovskite	*Pbnm*	20.5	4.855(1)	5.039(1)	7.187(2)	43.96(1)	Fe1: 0.5 0 0.5 0.05(1); Fe2: 0.5027(9) 0.5304(38) 0.25 0.04(1); O1: 0.076(17) 0.366(17) 0.25 0.13(3); O2: 0.171(10) 0.232(5) 0.561(19) 0.097(25)
37.3(4)	298	Rh_2O_3-II	*Pbna*	4.9	4.823(1)	5.009(1)	7.161(4)	43.25(1)	Fe: 0.7547(6) 0.0323(8) 0.1174(5) 0.040(3); O1: 0.596(7) 0.112(1) 0.843(2) 0.076(7); O2: 0.084(5) 0.25 0 0.070(1)
37.3(4)	298	Orthorombic perovskite	*Pbnm*	17.6	4.823(1)	5.009(1)	7.161(4)	43.25(1)	Fe1: 0.5 0 0.5 0.03(1); Fe2: 0.502(2) 0.549(12) 0.25 0.04(1); O1: 0.141(8) 0.424(12) 0.25 0.02(1); O2: 0.215(7) 0.230(12) 0.583(3) 0.02(1)

Table 3. Results of single-crystal structural refinement of $(Mg_{0.62}, Fe_{0.38})(Al_{0.36}Si_{0.64})O_3$ silicate perovskite (space group *Pbnm*) at different pressures and temperatures ($A = (Mg_{0.62}Fe_{0.38})$, $B = (Si_{0.64}Al_{0.36})$).

			Lattice parameters				
P (GPa)	*T* (K)	R1 (%)	*a* (Å)	*b* (Å)	*c* (Å)	*V* (Å^3/unit cell)	Atomic parameters (*xyzU*)
0.001	298	3.2	4.8110(4)	5.0007(3)	7.0293(3)	169.113(16)	A: 0.5161(3) 0.5604(3) 0.25 0.0089(7); B: 0.5 0 0.5 0.0056(8); O1: 0.1135(11) 0.4561(7) 0.25 0.009(1); O2: 0.1924(6) 0.1973(5) 0.5589(3) 0.010(9)
4.80(5)	298	2.9	4.7813(4)	4.9761(3)	6.9779(5)	166.022(20)	A: 0.5165(3) 0.5605(4) 0.25 0.0088(9); B: 0.5 0 0.5 0.0060(9); O1: 0.1127(13) 0.4553(8) 0.25 0.0079(12); O2: 0.1922(7) 0.1977(6) 0.5587(4) 0.0107(11)
9.88(5)	298	3.2	4.7533(2)	4.947(2)	6.9267(3)	162.886(11)	A: 0.5156(4) 0.5610(6) 0.25 0.015(1); B: 0.5 0 0.5 0.012(1); O1: 0.1139(16) 0.4572(10) 0.25 0.020(2); O2: 0.1907(10) 0.1949(8) 0.5591(5) 0.019(2)
17.8(1)	298	4.6	4.7227(6)	4.9164(4)	6.8810(6)	159.768(29)	A: 0.5168(4) 0.5622(7) 0.25 0.029(1); B: 0.5 0 0.5 0.025(2); O1: 0.1147(19) 0.4571(13) 0.25 0.036(2); O2: 0.1864(11) 0.1934(10) 0.5581(7) 0.035(2)
21.1(1)	298	6.6	4.7060(8)	4.8889(7)	6.8341(6)	157.23(4)	A: 0.5139(4) 0.5606(5) 0.25 0.041(1); B: 0.5 0 0.5 0.037(1); O1: 0.1139(20) 0.4628(13) 0.25 0.065(2); O2; 0.1838(13) 0.1930(7) 0.5570(6) 0.047(2)
29.5(2)	298	6.2	4.6579(9)	4.8665(5)	6.7711(8)	153.49(4)	A: 0.5154(13) 0.5660(10) 0.25 0.042(2); B: 0.5 0 0.5 0.048(3); O1: 0.1189(40) 0.4661(26) 0.25 0.053(4); O2: 0.1806(30) 0.1938(18) 0.5555(12) 0.053(4)
36.2(3)	298	6.1	4.6168(10)	4.8504(6)	6.7317(8)	150.75(4)	A: 0.5165(11) 0.5634(10) 0.25 0.043(2); B: 0.5 0 0.5 0.041(2); O1: 0.1205(40) 0.4640(30) 0.25 0.065(5); O2 0.1803(30) 0.1895(15) 0.5549(15) 0.047(3)
41.5(3)	298	4.6	4.5889(9)	4.8384(8)	6.7000(8)	148.76(4)	A: 0.5156(9) 0.5697(8) 0.25 0.053(2); B: 0.5 0 0.5 0.058(2); O1: 0.1238(30) 0.4634(22) 0.25 0.073(3); O2: 0.1806(20) 0.1857(11) 0.5558(11) 0.057(2)
42.0(3)	298	6.9	4.6046(9)	4.8269(4)	6.6802(7)	148.47(4)	A: 0.5201(11) 0.5682(13) 0.25 0.042(3); B: 0.5 0 0.5 0.039(3); O1: 0.1228(39) 0.4604(26) 0.25 0.052(4); O2: 0.1734(32) 0.1887(15) 0.5548(13) 0.046(4)
50.7(4)	298	9.2	4.5659(8)	4.7964(3)	6.6454(6)	145.53(3)	A: 0.5160(12) 0.5702(10) 0.25 0.047(2); B: 0.5 0 0.5 0.042(2); O1: 0.1247(35) 0.4674(30) 0.25 0.074(5); O2: 0.1751(26) 0.1865(14) 0.5556(12) 0.047(3)
54.6(4)	298	7.8	4.5454(6)	4.7971(3)	6.6273/5)	144.51(2)	A: 0.5191(10) 0.5678(13) 0.25 0.039(2); B: 0.5 0 0.5 0.034(3)O1 0.1226(40) 0.4605(30) 0.25 0.062(4); O2: 0.1682(27) 0.1879(14) 0.5535(13) 0.042(3)

(*Continued*)

Table 3. Continued.

			Lattice parameters				
P (GPa)	*T* (K)	R1 (%)	*a* (Å)	*b* (Å)	*c* (Å)	*V* (Å^3/unit cell)	Atomic parameters (*xyzU*)
62.9(4)	298	8.4	4.5049(7)	4.7646(5)	6.5765(5)	141.16(3)	A: 0.5161(18) 0.5701(14) 0.25 0.041(4); B: 0.5 0 0.5 0.046(4); O1: 0.1224(40) 0.4581(30) 0.25 0.037(5); O2: 0.1730(60) 0.1858(30) 0.5560(18) 0.055(5)
70.5(5)	298	6.5	4.4772(6)	4.7462(5)	6.5457(5)	139.10(3)	A: 0.5209(10) 0.5698(9) 0.25 0.059(2); B: 0.5 0 0.5 0.059(2); O1: 0.1195(19) 0.4570(18) 0.25 0.080(4); O2: 0.1708(20) 0.1848(12) 0.5565(10) 0.082(4)
72.5(5)	298	4.2	4.4767(4)	4.7375(4)	6.5320(4)	138.54(2)	A: 0.5196(9) 0.5666(7) 0.25 0.057(1); B: 0.5 0 0.5 0.058(1); O1: 0.1225(23) 0.4603(16) 0.25 0.065(3); O2: 0.1696(18) 0.1850(10) 0.5569(10) 0.060(2)
74.5(5)	298	6.7	4.4769(8)	4.7271(7)	6.5282(6)	138.16(4)	A: 0.5197(11) 0.5721(13) 0.25 0.034(3); B: 0.5 0 0.5 0.035(3); O1: 0.1191(60) 0.4632(27) 0.25 0.045(5); O2; 0.1717(44) 0.1866(17) 0.5572(11) 0.033(3)
76.3(5)	298	8.0	4.4562(6)	4.7250(4)	6.5143(4)	137.16(2)	A: 0.5181(5) 0.5684(6) 0.25 0.037(1); B: 0.5 0 0.5 0.042(1); O1: 0.1206(25) 0.4685(11) 0.25 0.039(2); O2: 0.1747(12) 0.1865(7) 0.5595(7) 0.037(2)
39.0(8)	2100(50)	6.4	4.6726(6)	4.8677(3)	6.7878(4)	154.39(3)	A: 0.5184(10) 0.5698(10) 0.25 0.062(2); B: 0.5 0 0.5 0.064(3); O1: 0.1207(47) 0.4634(26) 0.25 0.076(4); O2 0.1734(36) 0.1909(15) 0.5566(15) 0.073(4)
49.0(9)	2100(50)	8.3	4.6140(9)	4.8424(6)	6.7283(8)	150.33(3)	A: 0.5191(17) 0.5652(16) 0.25 0.048(3); B: 0.5 0 0.5 0.047(4); O1: 0.1229(48) 0.4591(30) 0.25 0.051(6); O2: 0.1708(35) 0.1884(19) 0.5543(21) 0.045(4)
63.1(9)	2050(50)	8.2	4.5604(5)	4.7942(3)	6.6395(6)	145.16(2)	A: 0.5201(10) 0.5662(16) 0.25 0.036(3); B: 0.5 0 0.5 0.032(3); O1: 0.1236(40) 0.4602(25) 0.25 0.046(4); O2: 0.1718(29) 0.1910(14) 0.5563(12) 0.038(4)
68.1(9)	1950(50)	6.1	4.5417(11)	4.7687(8)	6.6053(6)	143.06(4)	A: 0.5192(10) 0.5655(11) 0.25 0.075(2); B: 0.5 0 0.5 0.069(2); O1: 0.1213(26) 0.4587(23) 0.25 0.091(4); O2: 0.1706(28) 0.1912(15) 0.5569(12) 0.097(4)
79.5(1.0)	2050(50)	7.8	4.4854(5)	4.7638(7)	6.5735(5)	140.46(2)	A: 0.5194(15) 0.5677(14) 0.25 0.067(3); B: 0.5 0 0.5 0.064(3); O1: 0.1206(28) 0.4609(35) 0.25 0.090(6); O2; 0.1727(27) 0.1915(27) 0.5552(20) 0.089(6)
84.1(9)	2050(50)	8.0	4.4778(5)	4.7350(4)	6.5458(4)	138.79(2)	A: 0.5204(11) 0.5688(15) 0.25 0.049(3); B: 0.5 0 0.5 0.048(3); O1: 0.1183(47) 0.4594(34) 0.25 0.073(6); O2: 0.1714(35) 0.1893(17) 0.5547(12) 0.051(4)

larger, R1 = 20.5% (Table 2). The orthorhombic phase can be quenched at high pressures, and at 37.3(4) GPa and room temperature, 58 unique reflections were successfully collected, resulting in a discrepancy factor R1 = 4.9% for the Rh_2O_3-II-type structure and R1 = 17.6% for the orthorhombic perovskite structural model (Table 2). Thus, the single-crystal X-ray diffraction data unambiguously demonstrate that hematite transforms to the Rh_2O_3-II-type structured phase upon laser-heating at about 40 GPa. Although the reflections of the Rh_2O_3-II-type structure could be recorded on compression at ambient temperature up to at least 60 GPa, the quality of the crystals decreased with pressure and single-crystal structural refinements were therefore not performed.

4.3. *Structural behavior of silicate perovskite* $(Mg_{0.62},Fe_{0.38})(Al_{0.36}Si_{0.64})O_3$ *at conditions of the Earth lower mantle*

Iron and aluminum-bearing magnesium silicate perovskite (Mg, Fe, Si, Al)O_3 is the most abundant material on Earth because it is likely to be the main component of the lower mantle. For decades, the structure and properties of silicate perovskite have been the focus of mineral physics research, but so far single-crystal structural data are available only for its pure magnesium end-member $MgSiO_3$ perovskite at ambient temperature and pressures up to 10 GPa [27]. Iron and aluminum could significantly affect the properties of silicate perovskite, especially due to electronic transitions in Fe^{2+} and Fe^{3+} (see [28–30] and references therein). So far, only limited information based on powder X-ray diffraction data about the crystal-chemical effect of spin changes in ferrous iron is available [29,30]. Using a multi-anvil apparatus, we synthesized single crystals of $(Mg_{0.62},Fe_{0.38})(Al_{0.36}Si_{0.64})O_3$ silicate perovskite containing predominantly Fe^{3+} ($Fe^{2+}/\Sigma Fe \sim 7(3)\%$) and studied them in a DAC. Pressures reached 85 GPa at

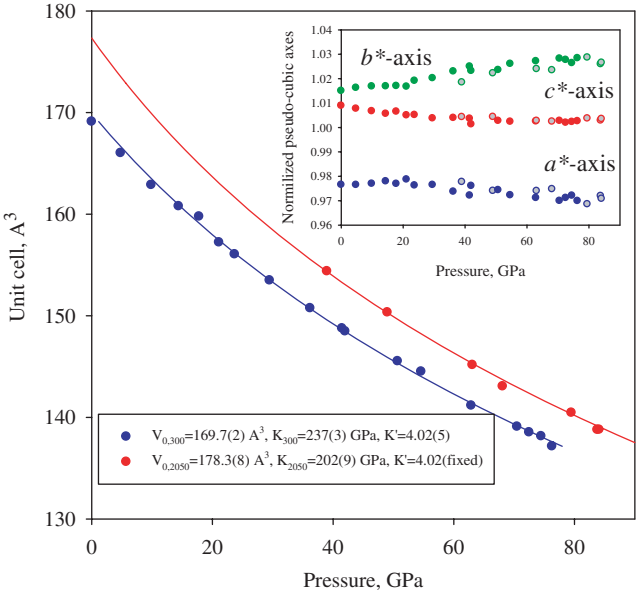

Figure 4. Pressure–volume equations of state of $(Mg_{0.62}, Fe_{0.38})(Al_{0.36}Si_{0.64})O_3$ silicate perovskite as obtained by means of single-crystal X-ray diffraction experiments in a laser-heated DAC. Uncertainties in the molar volume and in pressure (determined from the lattice parameters of Ne [23]) are within the symbols. Continuous curves are the fits of the experimental data using a third-order Birch–Murnaghan equation of state for ambient temperature (blue) and for 2050(100) K (red). The inset shows the variation with pressure and temperature (filled symbols, ambient temperature; open, 2050(100) K) of the normalized pseudo-cubic axes of orthorhombic perovskite ($a^* = a/\sqrt{2}\,(V/4)^{-1/3}$, $b^* = b/\sqrt{2}\,(V/4)^{-1/3}$ and $c^* = c/2\,(V/4)^{-1/3}$; a, b, c and V are the unit cell parameters and the cell volume, respectively) (color online).

ambient temperature and at 2050(100) K (Table 3). The sample was compressed at ambient temperature to about 30 GPa with steps of ∼4 GPa between the data-collection runs, and then heated to the desired temperature in the stability field of silicate perovskite. After each heating cycle, the laser power was gradually released, the pressure increased and the measurements were repeated. At each pressure–temperature point we were able to collect 50–70 unique reflections and refine the silicate perovskite structure to R1 below 8.5% (Table 3).

The fit of the molar volume data using a third-order Birch–Murnaghan equation of state (Figure 4) gives, for the P–V data collected at ambient temperature, the bulk modulus $K_{300} =$ 237(5) GPa, which is significantly lower than the bulk modulus of pure magnesium or Fe^{2+}-bearing silicate perovskite (250–264 GPa) [15,28,29]. The bulk modulus further decreases to 202(9) GPa at 2050(100) K (assuming the $K' = 4.02$ value obtained at ambient temperature). These results are in qualitative agreement with previous publications [15,28–30]. Similar to the behavior of ferrous silicate perovskite [28,29], the molar volume, lattice parameters (Figure 4), the mean bond distances of the (Si, Al)O_6 octahedra and (Mg, Fe)O_8 polyhedra (Figure 5) do not demonstrate any sign of irregular changes, which could be related to high-spin–low-spin

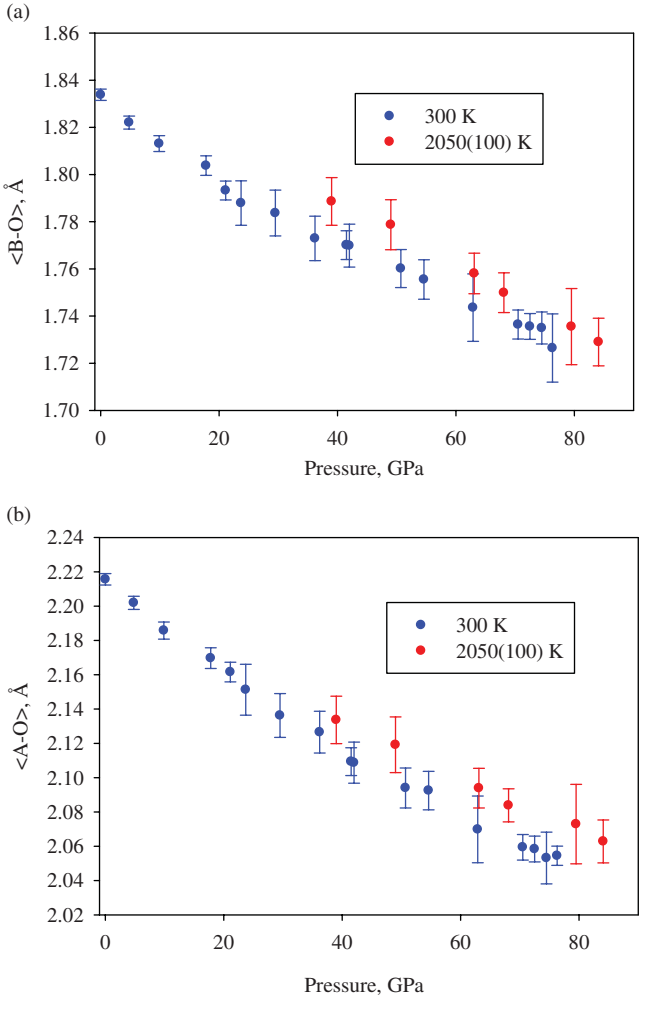

Figure 5. Pressure and temperature dependence of the mean bond distances of (Si, Al)O_6 octahedra (a) and of (Mg,Fe)O_8 polyhedra (b) in $(Mg_{0.62}, Fe_{0.38})(Al_{0.36}Si_{0.64})O_3$ silicate perovskite.

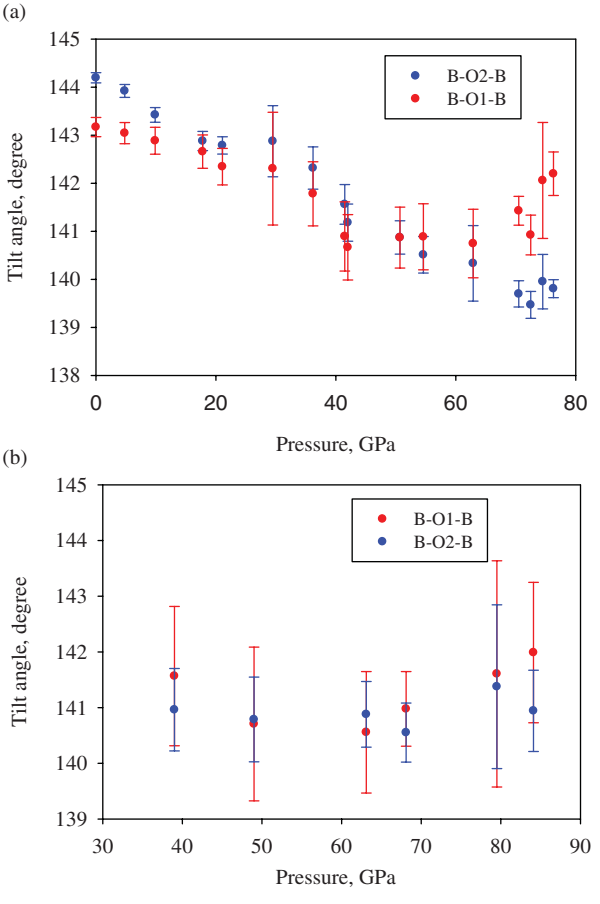

Figure 6. The variation of B–O1–B and B–O2–B (B=Si, Al) angles in $(Mg_{0.62}, Fe_{0.38})(Al_{0.36}Si_{0.64})O_3$ silicate perovskite with pressure and ambient temperature (a) and at 2050(100) K (b).

crossover [30]. However, close inspection of the variation of B–O1–B and B–O2–B tilt angles (B = Si, Al) with pressure (Figure 6(a)) shows that at ambient temperature above ~60 GPa the response of $(Si, Al)O_6$ octahedral network on compression changes. This effect may relate to the electronic transition in ferric iron reported by Catalli et al. [30] in the same pressure range. It is worth noting, however, that the high temperature, high pressure data relevant to conditions of the Earth's lower mantle (Figure 6(b)) do not show any changes in the compressional behavior of Fe^{3+}-bearing silicate perovskite at any pressure.

5. Conclusions

The examples above demonstrate that classical tasks of the solid state physics, material science and geoscience (like studies of thermal equations of state, determination and refinement of structures, investigations of properties and structures of materials at conditions of the Earth's and planetary interiors, etc.) can now be accomplished by means of single-crystal X-ray diffraction experiments at megabar pressures and temperatures of thousands of degrees. The application of the proposed methodology will not only make the use of single-crystal diffraction a routine tool for resolving structures at concurrent high pressure and high temperature, but can also be used for the direct

synthesis of materials at dozens of gigapascals in a laser-heated DAC and for *in situ* determination of their structure and crystal chemistry.

Acknowledgements

The authors appreciate useful discussions with J. Bock and A. Laskin and their technical assistance. Support from the ESRF and the DFG Priority Program 1236: "Strukturen und Eigenschaften von Kristallen bei extrem hohen Drücken und Temperaturen" is acknowledged.

References

[1] R. Boehler, *New diamond cell for single-crystal x-ray diffraction*, Rev. Sci. Instrum. 77 (2006), pp. 115103–115109.
[2] A. Friedrich, E. Haussuehl, R. Boehler, W. Morgenroth, E.A. Juarez-Arellano, and B. Winkler, *Single-crystal structure refinement of diaspore at 50 GPa*, Am. Mineralogist 92 (2007), pp. 1640–1644.
[3] E. Gregoryanz, L.F. Lundegaard, M.I. McMahon, C. Guillaume, R.J. Nelmes, and M. Mezouar, *Structural diversity of sodium*, Science 320 (2008), pp. 1054–1057.
[4] L.F. Lundegaard, E. Gregoryanz, M.I. McMahon, C. Guillaume, I. Loa, and R.J. Nelmes, *Single-crystal studies of incommensurate Na to 1.5 Mbar*, Phys. Rev. B. 79 (2009), p. 064105.
[5] F. Datchi, V.M. Giordano, P. Munsch, and A.M. Saitta, *Structure of carbon dioxide phase IV: breakdown of the intermediate bonding state scenario*, Phys. Rev. Lett. 103 (2009), pp. 185701–185705.
[6] M. Merlini, M. Hanfland, M. Gemmi, S. Huotari, L. Simonelli, and P. Strobel, *Fe^{3+} spin transition in $CaFe_2O_4$ at high pressure*, Am. Mineralogist 95 (2010), pp. 200–203.
[7] L. Wang, Y. Ding, W. Yang, W. Liu, Z. Cai, J. Kung, J. Shu, R.J. Hemley, W.L. Mao, and H.K. Mao, *Nanoprobe measurements of materials at megabar pressures*, Proc. Natl Acad. Sci. USA 107 (2010), pp. 6140–6145.
[8] M.E. Eremets, *High Pressure Experimental Methods*, Oxford Science Publications, 1996, p. 408.
[9] T.S. Duffy, *Synchrotron facilities and the study of the Earth's deep interior*, Rep. Prog. Phys. 68 (2005), pp. 1811–1859.
[10] R.J. Angel, J. Jackson, H. Reichmann, and S. Speziale, *Elasticity measurements on minerals: A review*, Eur. J. Minerol. 21 (2009), pp. 525–550.
[11] N. Dubrovinskaia and L. Dubrovinsky, *Whole-cell heater for the diamond anvil cell*, Rev. Sci. Instrum. 74 (2003), pp. 3433–3477.
[12] S. Klotz, J.-C., Chervin, P. Munsch, and G. Le Marchand, *Hydrostatic limits of 11 pressure transmitting media*, J. Phys. D: Appl. Phys. 42 (2009), p. 075413.
[13] A. Kurnosov, I. Kantor, T. Boffa-Ballaran, S. Lindhardt, L. Dubrovinsky, A. Kuznetsov, and B.H. Zehnder, *A novel gas-loading system for mechanically closing of various types of diamond anvil cells*, Rev. Sci. Instrum. 79 (2008), pp. 45110–45110.
[14] S.D. Jacobsen, C.M. Holl, K.A. Adams, R.A. Fischer, E.S. Martin, C. Bina, J.-F. Lin, V.B. Prakapenka, A. Kubo, and P. Dera, *Compression of single-crystal magnesium oxide to 118 GPa and a ruby pressure gauge for helium pressure media*, Am. Mineralogist 93 (2008), pp. 1823–1828.
[15] S.K. Saxena, L.S. Dubrovinsky, F. Tutti, and T. Le Bihan, *Equation of state of $MgSiO_3$ with the perovskite structure based on experimental measurement*, Am. Mineralogist 84 (1999), pp. 226–232.
[16] R.M. Hazen and L.W. Finger, *Comparative Crystal Chemistry: Temperature, Pressure, Composition and the Variation of Crystal Structure*, J. Wiley & Sons, London, 1982, p. 231.
[17] V.B. Prakapenka, A. Kubo, A. Kuznetsov, A. Laskin, O. Shkurikhin, P. Dera, M.L. Rivers, and S.R. Sutton, *Advanced flat top laser heating system for high pressure research at GSECARS: Application to the melting behavior of germanium*, High Press. Res. 28 (2008), pp. 225–235.
[18] W.A. Bassett, *The birth and development of laser heating in diamond anvil cells*, Rev. Sci. Instrum. 72 (2001), pp. 1270–1272.
[19] L. Dubrovinsky, K. Glazyrin, C. McCammon, O. Narygina, E. Greenberg, S. Uebelhack, A. Chumakov, S. Paskarelli, V. Prakapenka, J. Bock, and N. Dubrovinskaia, *Portable laser-heating system for diamond anvil cells*, J. Synchrotron Radiat. 16 (2009), pp. 737–741.
[20] G.M. Sheldrick, *A short history of SHELX*, Acta Cryst A 64 (2008), pp. 112–122.
[21] A. Dewaele, P. Loubeyre, and M. Mezouar, *Equations of state of six metals above 94 GPa*, Phys. Rev. B 70 (2004), p. 094112.
[22] S. Xiang, F. Xi, Y. Bi, J. Xu, H. Geng, L. Cai, F. Jing, and J. Liu, Ab initio *thermodynamics beyond the quasiharmonic approximation: W as a prototype*, Phys. Rev. B 81 (2010), p. 014301.
[23] Y. Fei, A. Ricolleau, M. Frank, K. Mibe, G. Shen, and V. Prakapenka, *Toward an internally consistent pressure scale*, Proc. Natl Acad. Sci. USA 104 (2007), pp. 9182–9186.
[24] M.P. Pasternak, G.Kh. Rozenberg, G. Machavariani, O. Naaman, R.D. Taylor, and R. Jeanloz, *Breakdown of the Mott–Hubbard state in Fe_2O_3: A first-order insulator–metal transition with collapse of magnetism at 50 GPa*, Phys. Rev. Lett. 82 (1999), pp. 4663–4668.
[25] S. Ono, T. Kikegawa, and Y. Ohishi, *High-pressure phase transition of hematite, Fe_2O_3*, J. Phys. Chem. Solids 65 (2004), pp. 1527–1530.

[26] S.H. Shim, A. Bengtson, D. Morgan, W. Sturhahn, K. Catalli, J. Zhao, M. Lerche, and V. Prakapenka, *Electronic and magnetic structures of the postperovskite-type Fe_2O_3 and implications for planetary magnetic records and deep interiors*, Proc. Natl Acad. Sci. USA 106 (2009), pp. 5508–5512.
[27] C.B. Vanpeteghem, J. Zhao, R.J. Angle, N.L. Ross, and N. Bolfan-Casanova, *Crystal structure and equation of state of $MgSiO_3$ perovskite*, Geophys. Res. Lett. 33 (2006), pp. L03306–L03310.
[28] S. Lundin, K. Catalli, J. Santillán, S.-H. Shim, V.B. Prakapenka, M. Kunz, and Y. Meng, *Effect of Fe on the equation of state of mantle silicate perovskite over 1 Mbar*, Phys. Earth Planet. Interiors 168 (2008), pp. 97–102.
[29] C. McCammon, I. Kantor, O. Narygina, J. Rouquette, U. Ponkratz, I. Sergueev, M. Mezouar, V.B. Prakapenka, and L. Dubrovinsky, *Stable intermediate-spin ferrous iron in lower-mantle perovskite*, Nat. Geosci. 1(10) (2008), pp. 684–687.
[30] K. Catalli, S.-H. Shim, V.B. Prakapenka, J. Zhao, W. Sturhahn, P. Chow, Y. Xiao, H. Liu, H. Cynn, and W. Evans, *Spin state of ferric iron in $MgSiO_3$ perovskite and its effect on elastic properties*, Earth Planet. Sci. Lett. 289 (2010), pp. 68–75.